

## DISCOVERY OF TWO GALAXIES DEEPLY EMBEDDED IN THE GREAT ATTRACTOR WALL

T. H. JARRETT

*Spitzer* Science Center, California Institute of Technology, Pasadena, CA, USA; jarrett@ipac.caltech.edu

B. S. KORIBALSKI

Australia Telescope National Facility, CSIRO, Epping, NSW, Australia

R. C. KRAAN-KORTEWEG AND P. A. WOUTD

Department of Astronomy, University of Cape Town, Rondebosch, Republic of South Africa

B. A. WHITNEY

Space Science Institute, Boulder, CO, USA

M. R. MEADE, B. BABLER, AND E. CHURCHWELL

Astronomy Department, University of Wisconsin-Madison, Madison, WI, USA

R. A. BENJAMIN

Physics Department, University of Wisconsin-Whitewater, Whitewater, WI, USA

AND

R. INDEBETOUW

Astronomy Department, University of Virginia, Charlottesville, VA, USA

*Received 2006 September 18; accepted 2006 November 3*

### ABSTRACT

We report on the discovery of two spiral galaxies located behind the southern Milky Way, within the least-explored region of the Great Attractor. They lie at  $(l, b) \approx (317^\circ, -0.5^\circ)$ , where obscuration from Milky Way stars and dust exceeds 13–15 mag of visual extinction. The galaxies were the most prominent of a set identified using mid-infrared images of the low-latitude ( $|b| < 1^\circ$ ) *Spitzer* Legacy program Galactic Legacy Infrared Mid-Plane Survey Extraordinaire. Follow-up H I radio observations reveal that both galaxies have redshifts that place them squarely in the Norma Wall of galaxies, which appears to extend diagonally across the Galactic plane from Norma in the south to Centaurus/Vela in the north. We report on the near-infrared, mid-infrared, and radio properties of these newly discovered galaxies and discuss their context in the larger view of the Great Attractor. The work presented here demonstrates that mid-infrared surveys open up a new window to study galaxies in the zone of avoidance.

*Key words:* galaxies: clusters: general — infrared: galaxies — radio lines: galaxies

### 1. INTRODUCTION

Our emerging portrait of the universe is that of an intricate cosmic web of galaxies arrayed in long filaments, sheets, and bubbles that intersect to form dense mass concentrations. The key outstanding problem is the distribution and nature of dark matter and dark energy that drives the dynamics of the expanding cosmos. The study of the local universe, including its peculiar motions and its clustering at the largest size scales, is essential for structure formation in the early universe and its relation to the formation and subsequent evolution of galaxies. Studying superclusters both near and far is paramount in decoding the mass density of the universe.

We now recognize that the core of one of the most important mass concentrations in the local universe is located behind the southern Milky Way ( $l \sim 320^\circ$ ,  $b \sim 0^\circ$ ). The so-called Great Attractor (GA) is pulling on the Milky Way and the Local Group of galaxies, its gravitational influence stretching beyond Virgo and the Local Supercluster of galaxies (Lynden-Bell et al. 1988; Burstein et al. 1990; Kocevski & Ebeling 2006; Erdogdu et al. 2006a, 2006b). The search for the elusive GA covers a very large expanse of sky that is within the zone of avoidance (ZoA), where traditional surveys are limited by the foreground Milky Way. It has been attributed to or associated with visible galaxy overdensities

in Hydra, Centaurus, Pavo, and Indus (e.g., Lahav 1987; Lynden-Bell et al. 1989), and most recently with dedicated surveys of the ZoA in Norma and Vela (e.g., see Kraan-Korteweg & Lahav [2000] and Kraan-Korteweg [2006] for reviews).

To date, the most prominent density peak to be discovered in the southern ZoA is the Norma Cluster (Abell 3627; Abell et al. 1989), whose cumulative mass and richness are comparable to the Coma Cluster (Kraan-Korteweg et al. 1996; Woudt et al. 1999). It is located below the southern Galactic equator ( $l = 325^\circ$ ,  $b = -7^\circ$ ,  $4900 \text{ km s}^{-1}$ ), the limit at which optical and near-infrared (NIR) surveys become heavily incomplete. To the north, emerging on the other side of the darkest region of the ZoA, are the Cen-Crux and CIZA J1324.7–5736 clusters, both at recessional velocities similar to that of Norma (Radburn-Smith et al. 2006). For a velocity range between 4000 and 6000  $\text{km s}^{-1}$ , a continuous line of galaxies appears to extend northward from Pavo-Indus up through Norma, bending to lower longitudes and joining with Cen-Crux/CIZA J1324.7–5736 in the northern Galactic hemisphere (see Fig. 1 in Jarrett 2004 for a three-dimensional view of these large-scale structures). This large filamentary structure, named the “Norma Wall,” runs diagonally behind the southern Milky Way (Kraan-Korteweg et al. 1994; Kraan-Korteweg 2006), severely hampering the construction of the sufficiently detailed large-scale flow maps that are needed to identify the full extent,

shape, and mass of the GA. Despite dedicated multiwavelength efforts in mapping the GA in the last decade (Kraan-Korteweg 2006), a complete census of the density and total mass is still unrealized.

From above the Earth's blocking atmosphere, the mid-infrared (MIR) opens a new and promising window for detecting ZoA galaxies. The MIR can penetrate the thick layer of Galactic gas and dust while being sensitive to both the stellar photospheric emission of early-type galaxies and the interstellar emission from star-forming late-type disk galaxies. The *Spitzer* Legacy project Galactic Legacy Infrared Mid-Plane Survey Extraordinaire (GLIMPSE; Benjamin et al. 2003) surveyed a large fraction of the Milky Way (within  $|b| < 1^\circ$ ) using the Infrared Array Camera (IRAC; 3.6–8  $\mu\text{m}$ ), passing across the most opaque part of the GA. GLIMPSE provides a readily available data set to test the viability of probing the ZoA with MIR imaging.

Inspection of the GLIMPSE MIR images revealed a number of galaxy candidates peeking through the formidable foreground of Galactic dust, gas, and stellar confusion. Intriguingly, a concentration of galaxy candidates appears to be projected against the Norma Wall exactly where the wall supposedly bends from the southern hemisphere to the northern hemisphere. To confirm their extragalactic nature, we have followed up two of the most promising galaxy candidates using deep NIR imaging (§ 2.2) and radio observations (§ 2.3). Both were found to have radial velocities that are consistent with membership in the Norma Wall (§ 3.2), thus providing compelling evidence that an extragalactic bridge exists between the southern and northern halves of the Galactic plane. In § 3 we report on the properties of these ZoA galaxies, and in § 4 we discuss their context in the larger view of the GA.

## 2. OBSERVATIONS AND DATA REDUCTIONS

### 2.1. *Spitzer* Mid-Infrared Observations

Active study of the Galactic plane is now underway with the *Spitzer Space Telescope*. The heart of the GA has been partially mapped by GLIMPSE using the *Spitzer* IRAC, covering the window between 3.6 and 8  $\mu\text{m}$ . The relatively shallow GLIMPSE images are comprised of two epochs of 2 s exposures, typically achieving a  $5\sigma$  surface brightness sensitivity of 2.7, 2.2, 6.3, and 5.6 mJy sr<sup>-1</sup> for the IRAC 3.6, 4.5, 5.8 and 8.0  $\mu\text{m}$  bands, respectively. The *Spitzer* GLIMPSE data reduction pipeline creates astrometric and photometric absolute-calibrated images that are combined into a single mosaic per band. The composite point source FWHM is  $\sim 2.5''$ .

At longer wavelengths, the MIPS GAL survey (S. Carey et al. 2007, in preparation) covered the same GLIMPSE footprint of the Milky Way using the Multiband Imaging Photometer for *Spitzer* (MIPS). The diffraction limit at 24  $\mu\text{m}$  is approximately  $6''$ , roughly a factor of 2 larger than the IRAC imaging, adequate for measuring the dust-emitting continuum from the GLIMPSE galaxies. A combined IRAC+MIPS panorama of the GA is shown in Figure 1, simultaneously illustrating the incredible beauty of the Milky Way and the major challenge we are faced with as we look behind the Galactic veil.

Visually scanning the set of GLIMPSE images that crossed the GA, we identified a number of resolved sources as promising extragalactic candidates for follow-up study. The two most prominent ones (see Fig. 1) lie at  $(\alpha, \delta)_{J2000.0} = (14^{\text{h}}48^{\text{m}}36.0^{\text{s}}, -60^{\circ}07'15'')$  ( $[l, b] = [317.04^\circ, -0.50^\circ]$ ) and  $(14^{\text{h}}47^{\text{m}}45.1^{\text{s}}, -60^{\circ}17'04'')$  ( $[l, b] = [316.87^\circ, -0.60^\circ]$ ), and are referred to as G 1 and G 2, respectively. These sources were found in relatively low 8 and 24  $\mu\text{m}$  background regions compared to the very bright

H II emission encircling the bubble-like clearing. The stellar confusion noise and the visual extinction, however, were extremely high, rendering both galaxies near the detection limit of GLIMPSE.

Photometry was extracted from the four IRAC bands and the MIPS 24  $\mu\text{m}$  image using a set of nested elliptical apertures centered on each galaxy, where the images were first cleaned of contaminating foreground stars. The background was determined using an annulus that was well outside of the galaxy light but still local to the galaxy environment and considerably smaller than the scale of the background interstellar medium gradients. For the IRAC measurements, the flux density of each source was aperture-corrected using the “extended source” prescription recommended by the *Spitzer* Science Center.<sup>1</sup> The expected uncertainty in the IRAC photometry (measurement errors plus calibration) is  $\sim 10\%$ . For the MIPS 24  $\mu\text{m}$  measurements, the appropriate aperture correction was determined to be  $\sim 1.1$  (see Fig. 3.2 of the MIPS data handbook), while another factor of 1.04 was applied to the integrated fluxes to account for the color correction between normal galaxies and the MIPS absolute calibration standard (see Table 3.12 in the MIPS data handbook). The expected uncertainty in the MIPS photometry is  $\sim 10\%$ – $15\%$ .

### 2.2. *Infrared Survey Facility* Near-Infrared Observations

NIR *JHK<sub>s</sub>* images of the region were obtained with the SIRIUS camera on the 1.4 m Infrared Survey Facility (IRSF) telescope (Glass & Nagata 2000; Nagayama et al. 2003) in South Africa during 2006 April 4 and 5. The exposures were relatively long, reaching the stellar confusion limit at 2  $\mu\text{m}$  for much of the region studied. The images were reduced by subtracting median “sky” images, then combined with astrometric and photometric calibration using Two Micron All Sky Survey (2MASS) stars in the field. The resulting mosaics, with  $\sim 0.9''$  FWHM profiles, were deep enough to detect the two GLIMPSE galaxies in all three NIR bands (see Fig. 1 inserts for combined NIR and MIR images). Photometry was extracted using the same set of elliptical apertures and methodology devised for the MIR images. The largest aperture corresponded to an isophotal surface brightness of 20.6 mag arcsec<sup>-2</sup>.

### 2.3. *Australia Telescope Compact Array* H I Observations

H I synthesis observations were obtained with the Australia Telescope Compact Array (ATCA) in the EW352 configuration on 2006 April 19 and 20. The pointing position was  $(\alpha, \delta)_{J2000.0} = (14^{\text{h}}48^{\text{m}}36^{\text{s}}, -60^{\circ}06'00'')$  ( $[l, b] = [317.05^\circ, -0.48^\circ]$ ). Since the galaxy redshifts were unknown but a connection with the GA anticipated, we observed with the large bandwidth of 16 MHz centered on 1397 MHz, leading to a velocity coverage ranging from  $\sim 3500$  to  $6000$  km s<sup>-1</sup>. With 512 channels the channel width was 6.7 km s<sup>-1</sup>. The field of view (primary beam FWHM) at 1397 MHz was 34.1'. The total observing time was  $\sim 12$  hr. We observed PKS 0823–500 and PKS 1934–638 for bandpass and flux calibration. The phase calibrator PKS 1338–58 was observed for 3 minutes every 40 minutes.

Data reduction was carried out with the MIRIAD software package using standard procedures. After identifying the velocity range of the H I signal we used the line-free channels to fit and subtract the radio continuum emission. Because of a strong confusing radio source, the H II region PMN J1445–5949,  $\sim 30'$  from the pointing center (upper right of Fig. 1), we used a third-order polynomial fit in *uvlin* to subtract the continuum emission. After Fourier transformation of the H I channel maps using “natural”

<sup>1</sup> See <http://ssc.spitzer.caltech.edu/irac/calib/extcal/>.

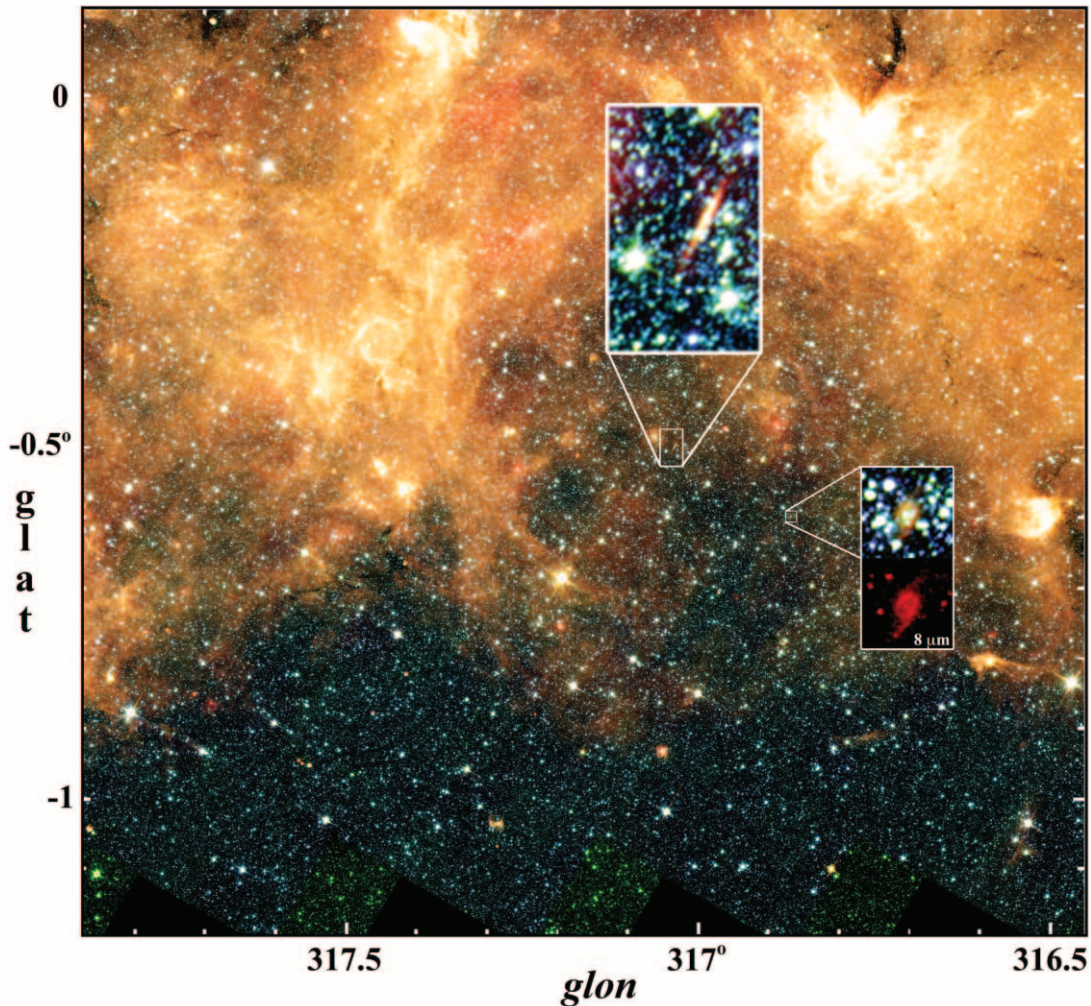


FIG. 1.—Infrared view of the heart of the Great Attractor region. This color composite of *Spitzer* IRAC (3.6  $\mu\text{m}$  [blue], 4.5  $\mu\text{m}$  [green], 5.8  $\mu\text{m}$  [yellow], and 8  $\mu\text{m}$  [orange]) and MIPS 24  $\mu\text{m}$  (deep red) images demonstrates the thick veiling due to stars, gas, and dust of the Milky Way. Nevertheless, the MIR penetrates deeply enough to reveal at least two galaxies that are shining through  $\sim 15$  mag of visual extinction. The inset images are constructed from deep IRSF  $JHK_s$  (1–2.2  $\mu\text{m}$ ) images combined with the MIR images. Note the extremely red colors of the edge-on disk galaxy G 1 (center) and the nearly face-on spiral galaxy G 2 (lower right), due to extreme dust reddening and the presence of strong PAH emission at 8  $\mu\text{m}$  (lower inset). The H I redshift is  $\sim 4500$  km s $^{-1}$  for both galaxies, placing them squarely in the Norma Wall of the GA.

weighting, the images were cleaned and restored with a synthesized beam of  $144'' \times 114''$ . The measured rms noise per 20 km s $^{-1}$  wide channel was  $\sim 2$  mJy beam $^{-1}$ .

### 3. RESULTS

#### 3.1. Infrared Emission and Foreground Extinction

The dust-obscured GLIMPSE galaxies are only visible at wavelengths longward of 1  $\mu\text{m}$ , significantly reddened due to selective extinction. We estimate the Galactic extinction using three independent techniques: dust column density, stellar colors, and galaxy colors. (In § 3.2 we estimate the foreground extinction using the radio and photometric properties combined with the Tully-Fisher [T-F] relation.) The goal is to arrive at a consistent value of the extinction that arises from the edge-on disk of the Milky Way. An accurate extinction correction will enable full characterization of the ZoA galaxies.

Far-infrared (FIR) emission, as measured by the *IRAS* and *COBE* space telescopes, can be used as an effective proxy of the dust column density of the Milky Way. The average dust extinction as inferred from the *IRAS*/DIRBE FIR maps (Schlegel et al. 1998) is  $A_V \sim 17.2$  and 17.7 mag, for G 1 and G 2, respectively.

The accuracy of these estimates is limited by the angular resolution and absolute calibration of the telescopes and detectors, as well as by confusion from Milky Way stars that are not associated with the interstellar dust column. Moreover, studies suggest that the FIR-inferred extinctions tend to be overestimated when the dust column density is large (e.g., molecular clouds; see, e.g., Arce & Goodman 1999; Nagayama et al. 2004; Schröder et al. 2005).

Shifting to the stellar population of the Galactic plane, field stars can be exploited at shorter wavelengths to infer the extinction by analyzing the red giant branch of the stellar color-magnitude diagram (CMD). Accordingly, 2MASS NIR photometry of stars in the direction of the GA is used to construct the CMD; recent examples using this method include Ferraro et al. (2006), Nishiyama et al. (2006), Rocha-Pinto et al. (2006), López-Corredoira et al. (2005), and Salaris & Girardi (2005). The 2MASS  $JHK_s$  CMD toward ( $l = 317^\circ$ ,  $b = -0.6^\circ$ , radius =  $0.3^\circ$ ) clearly separates into a distinct dwarf and red-clump sequence, as well as a strong bright red tail of reddened giants. The red clump extends to a distance of  $5.5 \pm 0.5$  kpc and has  $A_V = 8 \pm 1$  mag using red-clump intrinsic properties  $K = -1.5$  mag,  $J - K = 1.3$  mag (Bonatto et al. 2004; Salaris & Girardi 2002), and

TABLE 1  
INFRARED PHOTOMETRY OF THE GALAXIES G 1 AND G 2

$\lambda$ ( $\mu\text{m}$ )	GLIMPSE G 1 <sup>a</sup>			GLIMPSE G 2 <sup>b</sup>		
	Integrated Flux (mag)	Flux Density (mJy)	$\nu L_\nu$ ( $10^9 L_\odot$ )	Integrated Flux (mag)	Flux Density (mJy)	$\nu L_\nu$ ( $10^9 L_\odot$ )
1.25.....	10.80 $\pm$ 0.05	76.3 $\pm$ 0.1	20.4	<18	<0.1	0.02
1.64.....	10.08 $\pm$ 0.03	94.7 $\pm$ 0.3	19.8	10.67 $\pm$ 0.04	55.4 $\pm$ 0.3	11.6
2.15.....	9.91 $\pm$ 0.02	72.1 $\pm$ 0.7	11.2	10.54 $\pm$ 0.02	40.5 $\pm$ 0.5	6.29
3.6.....	9.76	35.0	3.25	10.47	18.3	1.70
4.5.....	9.68	24.1	1.79	10.38	12.7	0.94
5.8.....	8.01	71.8	4.13	8.99	29.1	1.68
8.0.....	6.41	175.7	7.33	7.66	55.6	2.32
23.7.....	4.20	153.2	2.13	5.07	68.5	0.95

NOTES.—Except for 24  $\mu\text{m}$ , all magnitudes and flux densities have been corrected for Milky Way dust extinction and internal extinction. The errors account for the photometry only, not for the applied foreground extinction corrections. IRAC and MIPS measurements have been aperture-corrected using the extended source prescription given by the *Spitzer* Science Center; typical uncertainties are  $\sim 10\%$ . The redshift-derived distance for both galaxies is 61 Mpc.

<sup>a</sup> At ( $l = 317.04^\circ$ ,  $b = -0.50^\circ$ ),  $a = 33.6''$ ,  $b/a = 0.25$ ,  $\phi = -50^\circ$ , and  $A_V = 15.1$  mag.

<sup>b</sup> At ( $l = 316.87^\circ$ ,  $b = -0.60^\circ$ ),  $a = 20.4''$ ,  $b/a = 0.55$ ,  $\phi = -43^\circ$ , and  $A_V = 13.0$  mag.

$A_V/A_K = 8.8$  (Draine 2003). This likely corresponds to the Scutum-Crux arm at about that distance and direction; however, the red clump is unlikely to be able to trace the full extent of the disk at 2MASS resolution and sensitivity. The bright giants are the only population that can reliably show the full extent of the Galactic disk at 2MASS sensitivity and resolution. Assuming constant NIR color for that population reveals a red giant branch extending to a dereddened  $K$  magnitude of  $\simeq 11.75$  mag, and a maximum (95th percentile) extinction  $A_V = 14 \pm 1$  mag. So between the FIR emission and the colors of field giants, the foreground extinction is estimated to be 14–17 mag in  $A_V$ .

Finally, the galaxy colors themselves can be used to estimate the foreground extinction. For galaxies in the local universe, the NIR window is sensitive to the old stellar population, regardless of Hubble type, whose photospheric light dominates the spectral energy distribution (SED) between 1 and 2  $\mu\text{m}$ . Consequently, the NIR colors of all types of galaxies are nearly identical (e.g., Jarrett 2000). Comparing the observed NIR colors with the expected colors yields an estimate of the color reddening, and hence the line-of-sight extinction. Accordingly, we have constructed the galaxy SEDs from the NIR and MIR measurements, which are directly compared with the expected light distribution of an old galaxy ( $t = 13$  Gyr) constructed from the GRASIL population synthesis (Silva et al. 1998). The model galaxy is weighted heavily to fit the peak in the SED light between 1 and 2  $\mu\text{m}$ , with lower weighting applied to the window between 3 and 5  $\mu\text{m}$  (where the presence of hot dust continuum and star formation line emission are beginning to become important). Extinction is a free parameter in the fit. The resulting best-fit SED corresponds to a total visual extinction (with  $A_V/A_K = 8.8$ ) of  $A_V = 15.1$  and  $13.0 \pm 0.2$  mag for the respective galaxies. We can estimate the internal extinction contribution using the measured axis ratio and the prescription from Masters et al. (2003):  $A_k = 0.26 \log(a/b)$ , where  $b/a$  is the disk axis ratio. The axis ratios as measured with the deep NIR images (Table 1) suggest an internal visual extinction of  $\sim 1.4$  mag for G 1 and 0.6 mag for G 2 at visual wavelengths. Hence, the total foreground extinction is  $A_V = 13.7$  and  $12.4 \pm 0.2$  mag for the respective galaxies. These SED-derived results are in good agreement with the CMD-derived values, and are within  $\sim 20\%$ – $30\%$  of the *IRAS*/*DIRBE* values. As noted above, the *IRAS*/*DIRBE* values have a larger uncertainty, and a potential systematic, in the Galactic plane. Next, in  $\S 3.2$  we show

that the inferred extinction based on the T-F luminosity is consistent with the CMD- and SED-derived estimates.

Using the SED-derived extinction for each galaxy G 1 and G 2, the corrected infrared photometry is summarized in Table 1, including the aperture parameters used to extract the photometry. Extinction corrections were carried out for the NIR and MIR photometry, except for the 24  $\mu\text{m}$  results, whose photometric measurement uncertainties were larger than the actual extinction correction appropriate to this long wavelength. Formal uncertainties in the measured fluxes ranged between 2% and 6% in the NIR, and  $\sim 10\%$  and 15% for the IRAC and MIPS measurements. The MIR uncertainty is dominated by the absolute calibration and the foreground stellar contamination, both arising from the significant scattering of stellar light across the IRAC focal planes. Due to the heavy foreground contamination from faint stars that we were unable to identify and remove, systematic overestimation of integrated fluxes cannot be discounted at the 5% level. Figure 2 shows the extinction-corrected SEDs for both

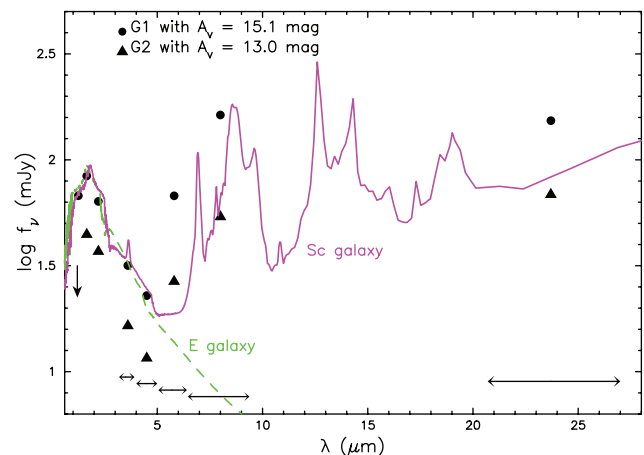


FIG. 2.—Infrared SED  $f(\lambda)$  of the galaxies G 1 (circles) and G 2 (triangles). The flux density for each measurement has been corrected for selective extinction ( $A_V = 15.1$  and 13.0 mag, respectively). For illustration, two SED templates are fitted to G 1: (1) an old 13 Gyr E-type galaxy (green dashed line), whose light is dominated by stellar photospheric emission from K/M giants, and (2) an Sc-type galaxy (magenta solid line), whose MIR light is dominated by strong PAH emission bands. The broad IRAC and MIPS bandpasses are indicated at the bottom.

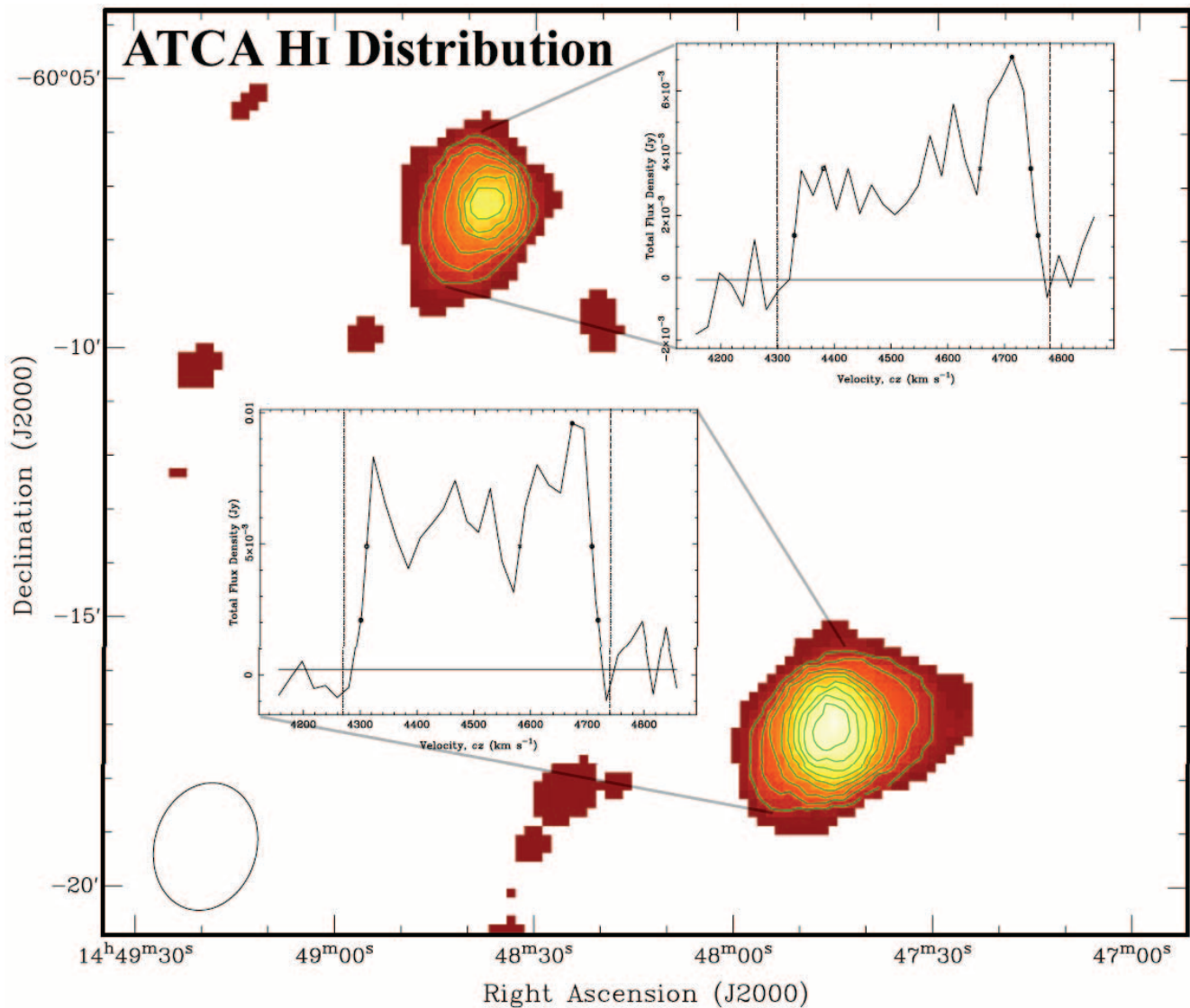


FIG. 3.—ATCA H I distribution map (moment 0) for the newly discovered galaxies G 1 (*upper*) and G 2 (*lower*), before primary beam correction. The synthesized beam ( $144'' \times 114''$ ; “natural” weighting) is displayed at the bottom left. The two insets show the corresponding integrated H I spectra. The two galaxies are separated by  $\sim 12'$  or  $\sim 200$  kpc (assuming a distance of  $D = 61$  Mpc).

galaxies. For clarity we only show the GRASIL model template fit to G 1, but note that G 2 also has a shape that fits the “old galaxy” template in the NIR portion of the SED. For comparison we also show the MIR model spectrum of a dusty Sc-type galaxy. In the MIR the galaxy emission significantly deviates from the Rayleigh-Jeans tail due to the presence of strong polycyclic aromatic hydrocarbon (PAH) emission at  $6.2$  and  $7.7 \mu\text{m}$ , boosting the IRAC  $5.8$  and  $8.0 \mu\text{m}$  bands. The strong PAH lines are consistent with active or ongoing star formation. Thermal dust continuum is also very strong in these galaxies as traced by  $24 \mu\text{m}$  light, consistent with a large reservoir of gas to fuel star formation (see below). The combined NIR+MIR images reveal G 1 to be an edge-on disk galaxy with a weak nucleus/bulge, akin to Sc/Sd types, while G 2 has a more face-on spiral orientation with a hint of large-scale bar structure, possibly of SBbc type.

### 3.2. Atomic Hydrogen

A close-up view of the ATCA H I distribution map that is centered on the GLIMPSE galaxies is presented in Figure 3. Both galaxies are clearly detected in H I. After primary-beam correction

we measure H I flux densities of  $F_{\text{H I}} = 1.1$  and  $5.6 \text{ Jy km s}^{-1}$  for G 1 and G 2, respectively. Both galaxies have systemic velocities around  $4500 \text{ km s}^{-1}$  (see insets in Fig. 3), which in the Local Group frame corresponds to  $\sim 4320 \text{ km s}^{-1}$ , giving a distance of  $61 \text{ Mpc}$  ( $H_0 = 72 \text{ km s}^{-1} \text{ Mpc}^{-1}$ ) or a distance modulus of  $33.93 \text{ mag}$ . At this distance the H I flux densities correspond to H I masses of  $10^9$  and  $5 \times 10^9 M_\odot$ , i.e., typical values for star-forming spiral galaxies. The H I properties are listed in Table 2.

The mean H I velocity fields of both galaxies (not shown) indicate systematic gradients, consistent with regularly rotating disks. Due to the low angular resolution, the position angle (P.A.) values of the disks are difficult to determine. For galaxy G 1 (Fig. 3, *top inset*) we measure  $\sim 140^\circ$ . Its large velocity width,  $w_{20} = 429 \text{ km s}^{-1}$ , is consistent with the edge-on orientation seen in the infrared images (Fig. 1). Interestingly, the H I profile is quite lopsided, with the redshifted horn being considerably stronger. This is also reflected in the H I distribution, which shows an extension of redshifted velocity gas toward the southeast. A higher resolution H I peak flux distribution (not shown) also shows the flux maximum shifted toward the southeast of the galaxy. Overall,

TABLE 2  
 H I PROPERTIES

GALAXY NAME	H I MAX. POSITION		$v_{\text{hel}}$ (km s <sup>-1</sup> )	$w_{50}$ (km s <sup>-1</sup> )	$w_{20}$ (km s <sup>-1</sup> )	$F_{\text{H I}}$ (Jy km s <sup>-1</sup> )	$M_{\text{H I}}$ (10 <sup>9</sup> M <sub>⊙</sub> )	$M_K(\text{T-F})$ (mag)
	$\alpha$ (J2000.0)	$\delta$ (J2000.0)						
GLIMPSE G 1 .....	14 48 39	-60 07 20	4563	365	429	1.1	1	-23.9
GLIMPSE G 2 .....	14 47 45	-60 17 09	4508	397	418	5.6	5	-24.4

NOTE.—Units of right ascension are hours, minutes, and seconds, and units of declination are degrees, arcminutes, and arcseconds.

the H I distribution of G 1 appears slightly less extended than that of G 2. The P.A. of the G 2 disk is approximately  $-70^\circ$ , compared to  $-40^\circ$  as viewed in the infrared. The large velocity width,  $w_{20} = 418 \text{ km s}^{-1}$ , is surprising given its rather face-on morphology in the infrared images, thus implying that the inclination-corrected line width is very large indeed. Finally, like G 1, the H I spectrum of G 2 appears to be asymmetric. In the higher resolution H I peak flux distribution, the H I maximum toward the south-eastern part of the galaxy (blueshifted velocities) is much stronger than that seen in the northwest (redshifted velocities).

With its favorable disk orientation, well-determined rotation velocity, and NIR flux, the absolute magnitude of galaxy G 1 can be estimated using the NIR T-F relation. We employ the  $K$ -band T-F relation constructed by Macri (2001), which correlates  $M_K$  with the inclination-corrected H I line width at the 20% level, calibrated with  $K$ -band isophotal integrated fluxes determined at the 21 mag arcsec<sup>-2</sup> level:

$$M_K = -22.53 - \{10.0[\log(w_{20}^i) - 2.5]\}.$$

The observed  $w_{20}$  line width is  $429 \text{ km s}^{-1}$ . The  $K$ -band axis ratio of G 1 is 0.25, corresponding to an inclination angle of  $81^\circ$ , assuming an intrinsic axis ratio of 0.2; hence, the  $1/\sin i$  correction to the line width is very small,  $\sim 1\%$ . Using a corrected line width  $w_{20}^i = 434 \text{ km s}^{-1}$ , the inferred absolute magnitude using the above T-F relation is  $-23.9 \text{ mag}$ , a luminosity that is  $\sim 2.5$  times brighter than  $L_*$  for the field disk galaxy population (Kochanek et al. 2001). We note that deriving  $M_K$  using other NIR T-F relations (e.g., Conselice et al. 2005) gives results that are in agreement to better than  $\sim 10\%$ . The redshift-based distance modulus is  $33.9 \text{ mag}$  (see above), which implies that the apparent  $K$ -band magnitude for G 1 should be about 10.0 mag. The 1.7 mag gap between this inferred apparent magnitude and the actual apparent magnitude, 11.72 mag (see § 3.1), represents the total extinction of Milky Way foreground plus G 1 internal. The resulting total extinction,  $A_v = 15.1 \text{ mag}$ , is remarkably close to the extinction deduced from the FIR dust emission and colors of field giant stars and of G 1 itself (see § 3.1). The clear implication is that G 1 follows the T-F relation that describes disk galaxies whose primary baryonic mass and H I components are intrinsic in origin.

Following the same exercise with G 2 is more problematic due to the relatively face-on disk inclination. The axis ratio implies an inclination that is  $60^\circ$ , or a  $1/\sin i$  correction that is  $\sim 15\%$ , leading to an inclination-corrected line width of  $483 \text{ km s}^{-1}$  and a T-F luminosity of  $-24.4 \text{ mag}$ . The inferred apparent  $K$ -band brightness is 9.6 mag, which in comparison to the actual  $K$ -band integrated brightness, 12.10 mag, implies a total extinction of greater than 20 mag at visual wavelengths. This value is much larger than what is inferred using the FIR, CMD, or G 2 SED, which suggests that G 2 does not follow the T-F relation, having a disk

rotation that is much greater than what is consistent with its  $K$ -band flux.

Taken as a whole, the large velocity width of G 2 and the lopsided H I distribution of both G 1 and G 2 (Fig. 3) may be hinting at a tidal distortion or a large-scale pressurized environment that is radially driving the H I gas from symmetry. Although the *Spitzer* IRSF and ATCA observations do not directly reveal any massive galaxies in the vicinity, we cannot discount the presence of H I-poor or old-star-dominated galaxies along this line of sight due to stellar confusion and the powerful nebular emission arising from the Milky Way (see e.g., the northern portion of Fig. 1). In any event, the intriguing H I line profiles merit further investigation.

#### 4. DISCUSSION AND SUMMARY

To summarize, we have detected several new galaxy candidates in the GA region using *Spitzer* MIR imaging from the GLIMPSE and MIPS GAL projects. Two of these sources were followed up with deep NIR imaging and H I line data, revealing that (1) both are relatively luminous star-forming galaxies rich with gas and dust, and (2) based on their H I radial velocities,  $\sim 4500 \text{ km s}^{-1}$ , they are located within the nominal confines of the GA. Previous X-ray, optical/NIR, and radio surveys of the GA did not detect these ZoA galaxies, and there is reason to believe that many more galaxies await discovery.

The region is extremely confused with gas, dust, and stars, limiting the short-wavelength surveys, while Galactic hydrogen emission hampers traditional single-dish blind surveys of nearby galaxies ( $< 500 \text{ km s}^{-1}$ ), and the increase in Galactic radio continuum sources at the lowest Galactic latitudes raises the noise level and reduces the effectiveness of 21 cm surveys. Galactic synchrotron radiation blinds searches for extragalactic radio continuum sources, and X-ray surveys are ineffective when the H I column density exceeds  $\sim (30-50) \times 10^{20} \text{ cm}^{-2}$  (Ebeling et al. 2002). Even with the *Spitzer* MIR imaging, we have found only a handful of galaxies peering through the formidable stellar/dust mask, although our follow-up multidish radio observations have proved to be very effective at penetrating the Galactic plane. Based on the T-F-derived luminosities, both GLIMPSE galaxies are brighter than typical field disk galaxies, so they may represent the upper tip of the luminosity function for field galaxies. Both have strong IR emission from star formation that does facilitate discrimination from the foreground stars using the NIR-to-MIR colors. The inferred foreground extinction,  $\sim 13-15 \text{ mag}$ , pushes the photometry near the detection limit for disk galaxies located at the distance of the Norma Cluster; consequently, most of the region studied is probably too opaque or confused with bright nebular emission to detect most background galaxies using the relatively shallow GLIMPSE data or the larger beam MIPS GAL data. Deeper *Spitzer* imaging complemented with multidish radio H I observations are what is needed to uncover fainter galaxies or sources that are cloaked by foreground stars and dust.

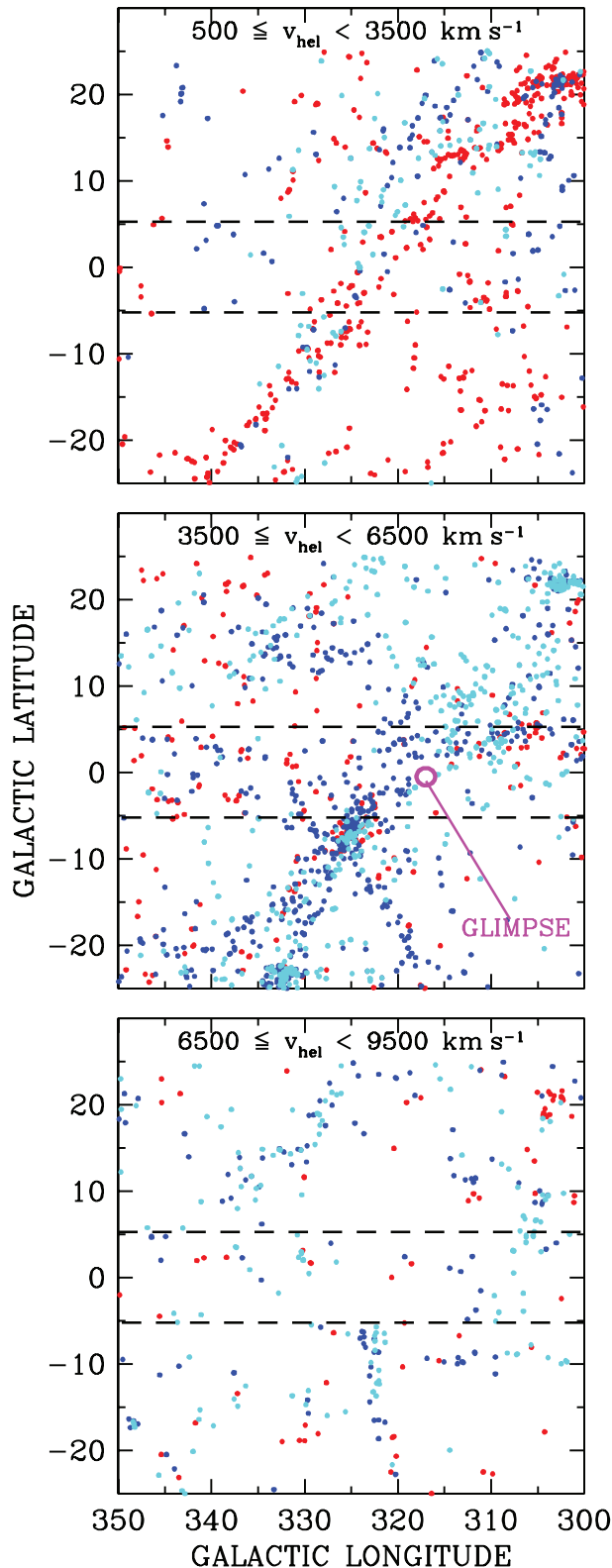


FIG. 4.—Wide-field depiction of galaxies in the GA. The three panels show galaxies with published radial velocities between 500 and 9500 km s<sup>-1</sup>, including data from the preliminary catalog of galaxies detected with the multibeam ZoA H I survey within  $|b| \leq 5^\circ$  (dashed lines; Kraan-Korteweg 2006), separated into bins that reveal the nearby Centaurus filament (top) and the more distant Pavo/Norma Wall (middle). In each panel the lowest velocities are denoted with cyan, moderate velocities with blue, and the highest velocities with red. The location of the GLIMPSE galaxies is denoted with a magenta circle in the middle panel.

Are the GLIMPSE galaxies tracing a larger concentration of galaxies that bridge the southern and northern hemispheres? Figure 4 depicts the emerging view of the GA and surrounding region, showing redshift-binned galaxy detections from X-ray, optical, NIR, and radio surveys. The GLIMPSE galaxies appear in Figure 4 (middle). At low redshifts,  $V_{\text{hel}} < 3500$  km s<sup>-1</sup> (Fig. 4, top), the less massive Centaurus Wall appears to extend from the southern to the northern hemispheres at a slight angle with respect to the supergalactic plane, whereas at higher redshifts, 3500–6500 km s<sup>-1</sup>, the combined filaments of the Pavo-Indus supercluster ( $l = 332^\circ$ ,  $b = -24^\circ$ , 4200 km s<sup>-1</sup>) and the Norma Cluster ( $l = 325^\circ$ ,  $b = -7^\circ$ , 4900 km s<sup>-1</sup>) in the south appear to pass through the GLIMPSE galaxies ( $l = 317^\circ$ ,  $b = -0.5^\circ$ , 4500 km s<sup>-1</sup>), bending to lower longitudes and higher velocities, joining up with the Cen-Crux Cluster ( $l = 306^\circ$ ,  $b = +5.5^\circ$ , 5700–6200 km s<sup>-1</sup>) and CIZA J1324.7–5736 ( $l = 307.4^\circ$ ,  $b = +5.0^\circ$ , 5700 km s<sup>-1</sup>) to the north.

The emerging portrait seems to be a continuous “great wall” that stretches from Pavo-Indus in the south ( $l \sim 340^\circ$ ), through Norma and upward (behind the Galactic plane) toward Centaurus, and finally bending over to Vela in the north ( $l \sim 270^\circ$ ), thus extending over  $\sim 50^\circ$ – $60^\circ$  on the sky. This astonishingly large structure is analogous to the Virgo-Coma Great Wall of galaxies discovered by the pioneering CfA redshift survey of the northern hemisphere (Geller & Huchra 1989). Such an extended mass concentration would surely perturb the Hubble flow of galaxies in the local universe ( $V_{\text{hel}} < 8000$  km s<sup>-1</sup>), deserving its “great” attractor status as surmised from large-scale flow studies of the last two decades (e.g., Kolatt et al. 1995). And indeed, recent all-sky coverage studies of the galaxy density field using X-ray-selected (Kocevski & Ebeling 2006) and NIR-selected (Erdogdu et al. 2006a, 2006b) galaxy samples clearly show the importance of the GA to the local velocity field. The GA is not the only attractor in the local universe; for example, the Perseus-Pisces supercluster is another important contributor to flow field, but it is the primary component within 8000 km s<sup>-1</sup>. At higher velocities, the Shapley Concentration at  $\sim 14,000$  km s<sup>-1</sup> is undoubtedly the most important structure in the local universe (Hudson et al. 2004; Kocevski & Ebeling 2006), although redshift and peculiar velocity studies are highly incomplete at these large distances. The density field studies implicate the GA as the primary perturbing force to the Local Group and the larger Local Supercluster, yet the detailed morphology of the GA remains to be understood. Combined MIR and radio surveys of the ZoA hold great promise in disentangling this cosmic web and delineating the Norma Wall from the foreground Milky Way.

Future work will include similarly targeted observations of new GLIMPSE and MIPS GAL galaxy candidates. Underway is a large-area, deep NIR survey with the IRSF, concentrating on the regions of the GA that have  $A_V < 10$  mag, complemented by more sensitive interferometric radio H I surveys that are optimized to finding galaxies in the velocity range of the Norma Wall. Finally, we will propose deeper *Spitzer* MIR imaging to probe the darkest regions of the ZoA.

We thank Sean Carey (*Spitzer* Science Center) for early access to the rich MIPS GAL data set, while Lucas Macri (NOAO) and Karen Masters (Cornell University) were a valuable Tully-Fisher resource. The contributions of the whole multibeam H I ZoA team are gratefully acknowledged, as well as of K. Wakamatsu and T. Nagayama of the IRSF survey team of the Norma Wall. R. K. K. and P. A. W. thank the National Research Foundation for financial

support. The Australia Telescope Compact Array is part of the Australia Telescope, which is funded by the Commonwealth of Australia for operation as a National Facility managed by CSIRO. The *Spitzer Space Telescope* is operated by the Jet Propulsion

Laboratory, California Institute of Technology, under contract with NASA. This research has made use of the NASA/IPAC Extragalactic Database, operated by IPAC/California Institute of Technology, under contract with NASA.

## REFERENCES

- Abell, G. O., Corwin, H. G., Jr., & Olowin, R. P. 1989, *ApJS*, 70, 1
- Arce, H. G., & Goodman, A. A. 1999, *ApJ*, 512, L135
- Benjamin, R., et al. 2003, *PASP*, 115, 953
- Bonato, C., Bica, E., & Girardi, L. 2004, *A&A*, 415, 571
- Burstein, D., Faber, S., & Dressler, A. 1990, *ApJ*, 354, 18
- Conselice, C. J., Bundy, K., Ellis, R. S., Brichmann, J., Vogt, N., & Phillips, A. 2005, *ApJ*, 628, 160
- Draine, B. T. 2003, *ARA&A*, 41, 241
- Ebeling, H., Mullis, C., & Tully, R. B. 2002, *ApJ*, 580, 774
- Erdogdu, P., Lahav, O., Huchra, J., Colless, M., & Jarrett, T. H. 2006a, *MNRAS*, 373, 45
- Erdogdu, P., et al. 2006b, *MNRAS*, 368, 1515
- Ferraro, F. R., Valenti, E., & Origlia, L. 2006, *ApJ*, 649, 243
- Geller, M., & Huchra, J. 1989, *Science*, 246, 897
- Glass, I. S., & Nagata, T. 2000, *Mon. Not. Astron. Soc. South Africa*, 59, 110
- Hudson, M. J., Smith, R., Lucey, J. R., & Branchini, E. 2004, *MNRAS*, 352, 61
- Jarrett, T. H. 2000, *PASP*, 112, 1008
- . 2004, *Publ. Astron. Soc. Australia*, 21, 396
- Kocevski, D. D., & Ebeling, H. 2006, *ApJ*, 645, 1043
- Kochanek, C. S., et al. 2001, *ApJ*, 560, 566
- Kolatt, T., Dekel, A., & Lahav, O. 1995, *MNRAS*, 275, 797
- Kraan-Korteweg, R. C. 2006, *Rev. Mod. Astron.*, 18, 48
- Kraan-Korteweg, R. C., Cayatte, V., Balkowski, C., Fairall, A. P., & Henning, P. A. 1994, in *ASP Conf. Ser. 67, Unveiling Large-Scale Structures behind the Milky Way*, ed. C. Balkowski & R. C. Kraan-Korteweg (San Francisco: ASP), 99
- Kraan-Korteweg, R. C., & Lahav, O. 2000, *A&A Rev.*, 10, 211
- Kraan-Korteweg, R. C., Woudt, P. A., Cayatte, V., Fairall, A. P., Balkowski, C., & Henning, P. A. 1996, *Nature*, 379, 519
- Lahav, O. 1987, *MNRAS*, 225, 213
- López-Corredoira, M., Cabrera-Lavers, A., & Gerhard, O. E. 2005, *A&A*, 439, 107
- Lynden-Bell, D., Faber, S. M., Burstein, D., Davies, R. L., Dressler, A., Terlevich, R., & Wegner, G. 1988, *ApJ*, 326, 19
- Lynden-Bell, D., Lahav, O., & Burstein, D. 1989, *MNRAS*, 241, 325
- Macri, L. M. 2001, Ph.D. thesis, Harvard Univ.
- Masters, K. L., Giovanelli, R., & Haynes, M. P. 2003, *AJ*, 126, 158
- Nagayama, T., et al. 2003, *Proc. SPIE*, 4841, 459
- . 2004, *MNRAS*, 354, 980
- Nishiyama, S., et al. 2006, *ApJ*, 647, 1093
- Radburn-Smith, D. J., Lucey, J. R., Woudt, P. A., Kraan-Korteweg, R. C., & Watson, F. G. 2006, *MNRAS*, 369, 1131
- Rocha-Pinto, H. J., Majewski, S. R., Skrutskie, M. F., Patterson, R. J., Nakanishi, H., Muñoz, R. R., & Sofue, Y. 2006, *ApJ*, 640, L147
- Salaris, M., & Girardi, L. 2002, *MNRAS*, 337, 332
- . 2005, *MNRAS*, 357, 669
- Schlegel, D. J., Finkbeiner, D. P., & Davis, M. 1998, *ApJ*, 500, 525
- Schröder, A., Kraan-Korteweg, R. C., Mamon, G. A., & Woudt, P. A. 2005, in *ASP Conf. Ser. 329, DENIS Detections of Highly Obscured Galaxies around PKS 1343–601*, ed. A. P. Fairall & P. A. Woudt (San Francisco: ASP), 167
- Silva, L., Granato, G., Bressan, A., & Danese, L. 1998, *ApJ*, 509, 103
- Woudt, P. A., Kraan-Korteweg, R. C., & Fairall, A. P. 1999, *A&A*, 352, 39